

CRITERIA FOR FLUX ROPE ERUPTION: NON-EQUILIBRIUM VERSUS TORUS INSTABILITY

P. DÉMOULIN AND G. AULANIER

LESIA, Observatoire de Paris, CNRS, 5 place Jules Janssen, 92190 Meudon, France; Pascal.Demoulin@obspm.fr

Received 2010 April 7; accepted 2010 June 8; published 2010 July 15

ABSTRACT

The coronal magnetic configuration of an active region typically evolves quietly for a few days before becoming suddenly eruptive and launching a coronal mass ejection (CME). The precise origin of the eruption is still under debate. The loss of equilibrium, or an ideal magnetohydrodynamic (MHD) instability such as torus instability are among the several mechanisms that have proposed to be responsible for the sudden eruptions. Distinct approaches have also been formulated for limited cases having circular or translation symmetry. We revisit the previous theoretical approaches setting them in the same analytical framework. The coronal field results from the contribution of a non-neutralized current channel added to a background magnetic field, which in our model is the potential field generated by two photospheric flux concentrations. The evolution on short Alfvénic timescale is governed by ideal MHD. We first show analytically that the loss of equilibrium and the stability analysis are two different views of the same physical mechanism. Second, we identify that the same physics is involved in the instabilities of circular and straight current channels. Indeed, they are just two particular limiting cases of more general current paths. A global instability of the magnetic configuration is present when the current channel is located at a coronal height, h , large enough so that the decay index of the potential field, $\partial \ln |\mathbf{B}_p| / \partial \ln h$, is larger than a critical value. At the limit of very thin current channels, previous analysis has found critical decay indices of 1.5 and 1 for circular and straight current channels, respectively. However, with current channels being deformable and as thick as that expected in the corona, we show that this critical index has similar values for circular and straight current channels, and is typically in the range [1.1, 1.3].

Key words: instabilities – magnetic fields – magnetohydrodynamics (MHD) – Sun: corona – Sun: coronal mass ejections (CMEs) – Sun: filaments, prominences – Sun: flares

1. INTRODUCTION

A coronal mass ejection (CME) is the consequence of a sudden destabilization of a part of the coronal magnetic field. The eruption is preceded by a long phase (days to week) during which the magnetic field is progressively stressed and free magnetic energy builds up. The configuration typically grows quasi-statically (with velocities well below the Alfvén velocity). At a certain point in the evolution, within a few minutes up to an hour, the system becomes very dynamic, with a global upward motion, as traced by the evolution of the cold plasma in the associated filament and of the hot plasma in coronal loops. Later on, a significant release of magnetic energy occurs and a flare is observed typically. If the downward magnetic tension of the covering magnetic arcade is weak enough, the erupting plasma and magnetic field are launched toward the interplanetary space as a CME. In summary, the CME phenomenon occurs in four main phases: buildup, instability, acceleration, and propagation. They have been reviewed by Forbes et al. (2006) and Vršnak (2008).

The last two phases are the most spectacular ones, and thus they are better constrained by observations and are more deeply modeled, in particular, with MHD simulations (e.g., Amari et al. 2003; Fan & Gibson 2007; Török & Kliem 2007). The first phase is a slow evolution, and it is usually difficult to characterize in observations the general key points that lead to eruption. The main physics that emerges from the observations is the presence of a new emerging magnetic flux, the progressive dispersion of the whole flux, the buildup of a very sheared field in the vicinity of the photospheric inversion line (PIL), and the cancellation of flux at the PIL (e.g., van Driel-Gesztelyi 1998; Green et al. 2002; van Driel-Gesztelyi et al. 2003). At the very least, the last three

are physically related since flux dispersion leads to convergent flows toward the PIL, increasing the magnetic shear, and forcing flux cancellation. This also implies the buildup of a flux rope with J-shaped coronal loops transformed by reconnection into S-shaped loops (e.g., Moore et al. 1995; Gibson et al. 2006; Green & Kliem 2009).

Why the magnetic configuration erupts is still an open issue. There is usually no evidence of a large amount of new magnetic flux (with a magnitude comparable to the pre-eruptive flux), and thus the eruption is not driven by the sub-photospheric evolution but rather, the coronal magnetic configuration becomes unstable at some point during the slow evolution. During this phase, magnetic reconnection is probably involved as a key mechanism for the progressive transformation of the magnetic configuration. However, an ideal instability is thought to initiate the CME since the upward acceleration phase starts before the impulsive phase of the flare in the majority of the events (e.g., Kahler et al. 1988; Maričić et al. 2007). Later on, magnetic reconnection plays a key role in the eruption as the peak of the upward acceleration is typically found to be correlated with the peak of the hard X-rays and of the time derivative of soft X-rays flux (e.g., Neupert et al. 2001; Zhang et al. 2001; Vršnak et al. 2004; Temmer et al. 2008).

Magnetic reconnection also plays a key role during the first phase as it permits the progressive transformation of very sheared field lines into a twisted flux rope. However, the MHD simulations of Aulanier et al. (2010) have shown that magnetic reconnection at the photospheric level, or later on in the corona below the flux rope, is not directly responsible for the onset of the eruption. The configuration rather gets unstable when the flux rope reaches a height where the potential field, associated with the distribution of the photospheric magnetic flux, is

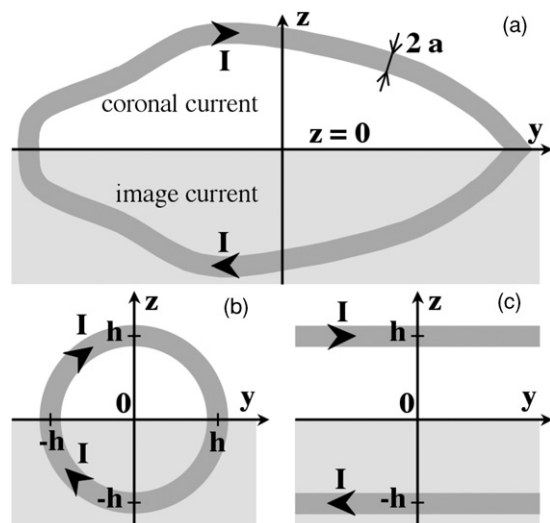


Figure 1. (a) Schema of a current channel in the corona and its image current below the photosphere (located at $z = 0$). The current channel has a radius a . (b) and (c) Particular cases with circular and straight current channels, respectively.

decreasing fast enough with height. This relates the onset of the eruption in MHD simulations to a series of analytical studies, as summarized below.

The equilibrium of a flux rope within a coronal field was first considered by Kuperus & Raadu (1974) with the following simplifications. In Cartesian coordinates, they modeled a flux rope with the magnetic field created by a straight line current of intensity I , located at a height $z = h$ above the photosphere, which is located at $z = 0$ (Figure 1(c)). The flux rope field is added to a simple background magnetic field: a potential field, \mathbf{B}_p , associated with a bipolar photospheric magnetic field. They included the observed *insignificant* evolution of the vertical component, B_z , at the photospheric level during the instability phase of a CME by introducing an image current of intensity $-I$, located at the height $z = -h$. The physical result is that two oppositely directed Laplace forces are acting on the coronal line current: one from the potential field \mathbf{B}_p and the other from the magnetic field created from the image current (or the equivalent surface current at $z = 0$). The equilibrium is then described by a curve $I(h)$.

van Tend & Kuperus (1978) showed that $I(h)$ is an increasing function of h at low height and that it has a local maximum if the horizontal component of \mathbf{B}_p orthogonal to the line current, $|B_{p,x}|$, decreases fast enough with height. Then, supposing that the current I can be progressively increased to larger values during the buildup phase, a loss of equilibrium occurs at $h = h_{\text{crit}}$, which is defined by the maximum of the function $I(h)$. This occurs where $|B_{p,x}|$ decreases faster than $1/h$. This model was later developed within a circuit theory, with an electric potential and a resistance introduced in the circuit to describe the temporal evolution of I . The current sheet that forms below the erupting flux rope was described by another electric circuit. This provided a set of coupled equations that describes the main phases of an eruptive flare (Martens & Kuin 1989; van Ballegoijen & Martens 1989). Next, the *background* potential field, \mathbf{B}_p , was replaced by a linear force-free field to include, as observed, a sheared field (Amari & Aly 1989). A loss of equilibrium is also present if $|B_{p,x}|$ is decreasing fast enough with height (Démoulin & Priest 1988).

In the above theory, it is supposed that the current intensity, I , is the main driver of the evolution and that it can be increased

to arbitrarily large values. However, the coronal physics is not precisely described by any circuit theory because the electric current is a consequence of the force balance together with MHD constraints (e.g., Parker 1996a). The effect of magnetic reconnection on the system (through changing field line connectivity and energy release) before the flare/CME acceleration phase is minimal and therefore the stability of an equilibrium is typically tested in ideal MHD. The conservation of the coronal magnetic flux passing below the flux rope is typically used to set a constraint on the current evolution. Anzer & Ballester (1990) claimed that there is no longer a loss of equilibrium with this ideal MHD constraint, but Démoulin et al. (1991) found that this constraint mostly displaced the loss of equilibrium point to a larger height (slightly after the maximum of the $I(h)$ curve), in agreement with the MHD simulation of Forbes (2000). The following developments have shown that a loss of equilibrium is typically present if the flux rope radius is thin enough. It occurs, for example, when the photospheric polarities are subject to converging motions toward the PIL, or when their magnetic flux is decreased, even when ideal MHD is assumed during the full buildup phase, (Isenberg et al. 1993; Forbes & Isenberg 1991; Forbes & Priest 1995).

When the current channel is curved, an extra force called the hoop force (e.g., Bateman 1978), is present. The electric current of a curved channel creates a magnetic field component orthogonal to the channel. This implies an outward Laplace force (away from the curvature center). In terms of the magnetic field, this force is due to a larger magnetic pressure of the azimuthal field component present on the side of the curvature center. This force is at the heart of the magnetically driven model of Chen (1989) and the subsequent developments of this model (e.g., Garren & Chen 1994; Krall et al. 2000). This force is also present in the MHD models where the straight line current mentioned previously is replaced by a ring of current (Lin et al. 1998, 2002; Titov & Démoulin 1999). As for the above Cartesian models, an ideal MHD evolution during the buildup phase typically also, but not always, leads to a loss of equilibrium. The differences will be discussed in Sections 3 and 4. A non-equilibrium point could also be present when line-tied conditions are imposed at the photospheric footpoints of the flux rope (Isenberg & Forbes 2007).

From another point of view, Kliem & Török (2006) studied the stability of a toroidal current ring immersed in a background potential field \mathbf{B}_p . Extending the results summarized in Bateman (1978), they derived that an instability occurs when the background field component orthogonal to the torus ($|B_{p,x}|$) decreases faster than $1/h^{3/2}$ with a correction depending on the torus aspect ratio (major over minor radius). Kliem & Török (2006) called it “torus instability.” They analyzed cases where the electric current I was held constant or fixed by the conservation of the total magnetic flux within the torus hole.

The aim of this present paper is to revisit the above studies to analyze their *relationships*. Is this “torus instability” different from the loss of equilibrium found in previous studies with a toroidal current? Does it have a different physical origin than the instability van Tend & Kuperus (1978) obtained with a straight current channel? The Cartesian and axisymmetric models are first written with the same formalism in Section 2. We compare the loss of equilibrium and the instability approaches in both geometries in Section 3, before comparing the criteria of instabilities taking into account a finite current-channel width that evolves during the perturbation (Section 4). Finally, in Section 5, we summarize our results and discuss the relationship

between the Cartesian and axisymmetric models, as well as the relationship between the loss of equilibrium and torus instability.

2. BASIC CONCEPTS

The coronal magnetic field \mathbf{B} can always be written as the sum of a background magnetic field \mathbf{B}_p and the magnetic field \mathbf{B}_l , which are created by localized coronal currents and their images below the photosphere (Section 2.2). \mathbf{B}_l has a vanishing B_z component at $z = 0$ by construction. All the analytical models use this field decomposition with various approximations for \mathbf{B}_l . \mathbf{B}_p is most frequently taken as the unique potential field associated with the photospheric “normal magnetogram” $B_z(x, y, 0)$ and with vanishing strength at infinite distance. We consider this case below; however, it is worth noting that, in general, \mathbf{B}_p can also incorporate distributed coronal currents (e.g., \mathbf{B}_p could be a linear force-free field and \mathbf{B}_l needs to be self-consistently computed; Démoulin & Priest 1988).

2.1. Modeling with Concentrated Currents

In order to solve the derived set of equations analytically, simplifications in the magnetic configuration need to be made. The first one is to suppose that the electric current is restricted to a thin channel in the corona (Figure 1(a)). More precisely, its typical thickness, $2a$, must be small compared to the spatial scales of \mathbf{B}_p and to the local radius of curvature of the current channel axis. In an active region, the magnetic shear is typically concentrated around the PIL, while the surrounding arcade has more potential, so the electric currents are stronger around and above the PIL. With reconnection of sheared loops at the PIL, a significant fraction of the currents is inside a twisted flux tube (Aulanier et al. 2010 and references therein). Thus, the introduction of a concentrated current channel is motivated by observations and MHD simulations; however, it is still an important simplification (e.g., neglecting the effect of more distributed currents as well as the presence of narrow current layers and sheets).

The *approximation* of a thin current channel allows us to separate approximately the magnetic equilibrium into an internal and external equilibrium (Chen 1989; Isenberg et al. 1993). This splitting is better achieved when the current channel is thin. For the external equilibrium, the Laplace force, integrated over the channel cross section vanishes, so that there is no average magnetic field component orthogonal to the current channel. The internal equilibrium is solved locally in the channel cross section.

A twisted flux tube generally has both toroidal (axial) and poloidal (azimuthal) magnetic field and electric current components. The equilibrium is typically solved in cylindrical coordinates with a balance between the total magnetic pressure gradient and the tension of the poloidal magnetic field (force-free field solution). This internal equilibrium is not the object of this paper and we refer the reader to the work of Lin et al. (1998) for information on this topic.

Another important simplification is the absence of a neutralization or return current around the direct current. Such return current, with a direction opposite to and with the same magnitude as the direct current, is expected to be present in a magnetic field formed by the emergence of a flux rope or deformed by localized boundary (photospheric) motions (Parker 1996b). In both cases, the complete neutralization is due to a vanishing circulation of \mathbf{B} around a large path enclosing the current chan-

nel. Return currents are indeed present in MHD simulations, but when a significant magnetic field component is present along the PIL, the direct current has a larger magnitude than the return current (Török & Kliem 2003; Aulanier et al. 2005). Indeed, only partial neutralization has typically been reported in sunspots (Wheatland 2000; Venkatakrishnan & Tiwari 2009). With partial neutralization, the current intensity, I , is the non-vanishing sum of the two opposite currents.

We argue that the occurrence of non-fully neutralized currents should be a common feature in solar active regions. The contrary would imply that current-carrying flux tubes should be fully surrounded by potential fields, not only high up in the corona, but also down low around the PILs. It is worth noting, however, that some MHD models for solar eruptions clearly do not require a net current (the magnetic breakout, tether cutting, and flux disappearance models, respectively addressed by Antiochos et al. 1999, Moore & Roumeliotis 1992, and Amari et al. 2000 as they are based on the gradual diminishing of the tension of the background field, irrespective of the distribution of electric currents at lower altitudes. Many other models exist (as reviewed e.g., in Forbes et al. 2006; Aulanier et al. 2010), but it is conceivable that several actually fall into the physical frame studied in the present paper.

2.2. Image Current

The lack of significant photospheric magnetic flux evolution during the initiation of a CME can be modeled with the introduction of image currents below the photosphere. The straight channel case of Kuperus & Raadu (1974) can be generalized to any channel shape as illustrated in Figure 1(a). Let the current vector be (I_x, I_y, I_z) at a generic point (x, y, z) in the corona. Then, the introduction of the image current $(-I_x, -I_y, I_z)$ at the image position $(x, y, -z)$ implies that the vertical component of the magnetic field at the photosphere, $B_z(x, y, 0)$ is unaffected by the presence of the current channel.

The introduction of this image current is a particular case of the technique of images imposing a particular boundary condition on the setting of electrodynamic problems (Jackson 1975, chaps. 2 and 5). Physically, the coronal current path is closing in a complex set of horizontal photospheric currents which create the same coronal magnetic field as the image current.

2.3. Magnetic Flux

Assuming that photospheric evolution and magnetic reconnection are negligible during the instability phase, the total coronal magnetic flux passing below the current channel is conserved. This flux is the sum of the flux of \mathbf{B}_p and \mathbf{B}_l . By the symmetric construction of the image current, the coronal flux of \mathbf{B}_l is half the flux enclosed by the full current channel (coronal and image current), and thus it is equal to $LI/2$, where L is the *external* inductance of the full current channel (e.g., Jackson 1975).

The total inductance of a circular channel of main radius h and of small radius a (Figure 1(b)) is

$$L_c = \mu_0 h \left(\ln \left(\frac{8h}{a} \right) - 2 + \frac{l_i}{2} \right), \quad (1)$$

where μ_0 is the magnetic permeability and l_i is the normalized internal inductance, per unit length, of the current channel (Grover 1946). l_i takes the value of 0, 0.5, or 1 for a current concentrated at the border of the torus, uniformly distributed

within the cross section, or with a linear force-free field equilibrium (Lin et al. 1998, and references therein), respectively. Equation (1) is simple but still a good approximation of more complete expressions. For example, it is close to the series expansion tabulated by Malmberg & Rosenbluth (1965) in the range $0.1 < a/h < 1$ for $l_i = 0$. Moreover, the expression with elliptic integrals given by Ramo et al. (1994, p. 193) is also close to Equation (1) with $l_i = 0$ in the range $0.15 \leq a/h < 1$, while for lower a/h values it is closer to the case $l_i = 0.5$. Finally, for the coronal magnetic flux passing below the current channel, the external inductance is required, so the flux is $L_c I/2$ with $l_i = 0$.

Using the same notations (Figure 1(c)), the total inductance of a straight channel and its image, for a length Δy along the channel, is

$$L_s = \frac{\mu_0 \Delta y}{\pi} \left(\ln \left(\frac{2h}{a} \right) + \frac{l_i}{2} \right), \quad (2)$$

where l_i has the same value as in the above circular case. The main difference with the circular case is that L_s is only weakly dependent on h so that L_s is almost constant during a global perturbation of the channel (modifying the height h). As described above, the coronal magnetic flux passing below the current channel is $L_s I/2$ with $l_i = 0$.

2.4. Magnetic Self Force

From the Biot and Savart law, the current channel generates a magnetic field at any point in space. The component of this field orthogonal to the current channel induces a Laplace force. The direct calculation of this force from the Biot and Savart law is very cumbersome even for a simple torus geometry. In practice, this force is computed by equating the work of this force to the change of the magnetic energy ($LI^2/2$) during an elementary displacement, preserving the magnetic flux encircled by the current channel, LI , so that there is no inductive effect (Shafranov 1966; Garren & Chen 1994). For a circular current channel, this implies an outward radial force f_c per unit length along the channel, given by

$$f_c = \frac{I^2}{2} \frac{\partial L_c}{\partial h} = I^2 \frac{\mu_0}{4\pi h} \left(\ln \left(\frac{8h}{a} \right) - 1 + \frac{l_i}{2} \right). \quad (3)$$

The force f_c is the Laplace force between the toroidal (axial) current and the poloidal magnetic field. There is also the Laplace force between the poloidal current and the toroidal magnetic field inside the twisted flux tube. Taking into account the internal equilibrium, in the limit $a/h \ll 1$, this second force only gives a small correction to the previous force, as the total force is obtained from Equation (3) by replacing l_i with $l_f = l_i - S_h$, with $S_h \approx 1$ (Shafranov 1966). Then, we write the total force as $r_c I^2$ with

$$r_c = \frac{\mu_0}{4\pi h} \left(\ln \left(\frac{8h}{a} \right) - 1 + \frac{l_f}{2} \right). \quad (4)$$

The local outward force $r_c I^2$, called the hoop force, has its origin in the magnetic field created by each of the elementary parts of the circular ring with the largest contribution coming from the closest currents. Indeed, it has a logarithmic divergence as the small radius a becomes smaller. For $a \ll h$, the logarithm term slightly dominates in Equation (4). If the current channel is fully in the corona (e.g., Lin et al. 1998), Equation (4) includes only the self-force of the coronal current channel, whereas if only half the current channel is in the corona (e.g., Lin et al. 2002, Figure 1(b)) Equation (4) also includes the force from the

image current. Finally, Garren & Chen (1994) have generalized these results to current channels with arbitrary shapes.

For a straight current channel, located at a height h above the photosphere, the magnetic force can be computed as above (Equation (3)) with L_c replaced by L_s or the magnetic field of the image current can be computed first by the Biot and Savart law. The repulsion function r_s is

$$r_s = \frac{\mu_0}{4\pi h}. \quad (5)$$

r_s indeed has a similar form as r_c (Equation (4)) since the logarithm term provides only a weak dependence on h/a .

3. LOSS OF EQUILIBRIUM AND INSTABILITY

3.1. Magnetic Field Evolution

The MHD evolution of the coronal magnetic field of an active region, outside flare times, typically has three timescales, as follows. The shortest timescale, τ_A , called the Alfvén time, is the typical time that Alfvén waves require to cross the coronal field configuration. Outside of the eruption period, the magnetic configuration does not significantly change on such a timescale and Alfvén waves transport the magnetic stresses (shear, twist). On the intermediate timescale, τ_B , the coronal magnetic stress is significantly changing, for example, because the sub-photospheric torsional Alfvén waves are bringing a twist to the coronal field, or because the reconnection between sheared magnetic loops is forced by converging flows at the PIL. On this intermediate timescale, coronal currents significantly change but not the global photospheric distribution of the magnetic field component normal to the photosphere (i.e., the “normal magnetogram”). On the longest timescale, τ_C , both the coronal currents and the “normal magnetogram” are evolving.

For a mature active region with a magnetic flux of $\approx 10^{22}$ Mx, the above timescales are typically of the order of $\tau_A \approx$ few minutes, $\tau_B \approx$ few days, and $\tau_C \approx$ week to months. They are well separated, a useful property for an analytical study since it allows one to isolate the main physics involved in each timescale. Thus, we can use different approximations to analyze the magnetic field evolution on these timescales, as follows. The global stability of the equilibrium can be tested with the ideal MHD on the shortest timescale τ_A . On the intermediate timescale τ_B , the buildup of coronal current can be studied within a given potential \mathbf{B}_p (computed uniquely from the “normal magnetogram,” using appropriate boundary conditions on the sides of the domain). Finally, the evolution on the longest timescale τ_C is mostly studied with MHD simulations or with analytical studies imposing an ideal-MHD evolution.

3.2. Loss of Equilibrium with a Circular Current Channel

First, we revisit the model proposed by Titov & Démoulin (1999), keeping it as simple as possible. The potential field \mathbf{B}_p is created by two magnetic sources of equal flux ϕ but of opposite signs, located at $x = \pm D$, $y = z = 0$, and by a line current located at $y = z = 0$. The magnetic field of this line current contributes to the coronal potential field, but it neither modifies the equilibrium nor the equilibrium perturbation studied below, so this field is not present in the following equations (the aim of this magnetic field is only to have a finite twist in the coronal field). A torus of electric current, centered at $x = y = z = 0$, is introduced in the plane $y-z$ (Figure 1(b)). Since the photospheric boundary is set at $z = 0$, the half part of the torus at $z < 0$ represents the image current.

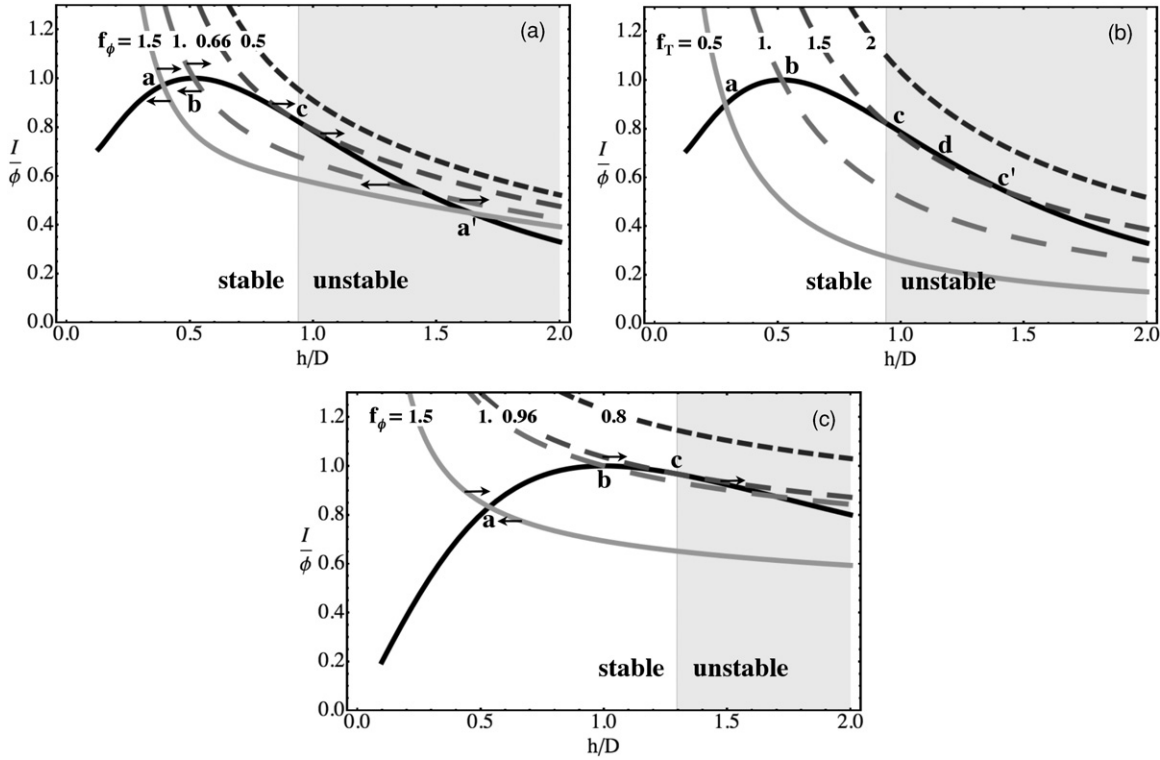


Figure 2. Coronal electric current, I , divided by the photospheric magnetic flux ϕ , as a function of the coronal height h , normalized to half the x distance, D , of the photospheric magnetic polarities. The equilibrium curve, $I_{\text{eq.}}/\phi(h)$, is in black, while the evolution constraint is shown in gray/dashed style for four values of the evolution factor f . Both f and $I_{\text{eq.}}/\phi$ are normalized to 1 at the maximum of $I_{\text{eq.}}/\phi$. (a) and (b) Case of a circular current channel (Figure 1(b)), (c) case of a straight current channel (Figure 1(c)). (a) and (c) The photospheric flux, ϕ , is evolved with the factor $f = f_\phi$. (b) The magnetic twist of the flux tube is evolved with the factor $f = f_T$. Arrows represent the direction of the force when the system is perturbed away from the equilibrium.

As the magnetic configuration considered is axisymmetric (around the x -axis), the magnetic force on the current channel is radial in the y - z plane with the same value along the current channel:

$$f = r_c I^2 + B_{p,x} I, \tag{6}$$

where r_c is given by Equation (4). The x -component of \mathbf{B}_p at the current location is

$$B_{p,x} = -4\phi D(h^2 + D^2)^{-3/2}. \tag{7}$$

The equilibrium current, $I_{\text{eq.}}$, is given by $f = 0$ in Equation (6):

$$I_{\text{eq.}}(h) = \frac{16\pi \phi D h (h^2 + D^2)^{-3/2}}{\mu_0 \ln(8h/a) - 1 + l_f/2}. \tag{8}$$

Starting from a nearly potential configuration (small I value), if the current value could be progressively increased as a function of time as in a classical electric circuit, a loss of equilibrium would occur when I would reach the maximum value of $I_{\text{eq.}}(h)$. The circular current channel behaves in the same way as a straight current channel and its image current (Figure 1(c) and Section 3.6) as proposed by van Tend & Kuperus (1978). However, with an MHD evolution, the magnitude of the coronal current is rather determined by the magnetic field evolution, so its time evolution cannot be imposed a priori. Indeed, during a typical MHD evolution with imposed photospheric velocities, the coronal current magnitude first increases then later decreases (e.g., Aly 1985; Klimchuk & Sturrock 1989; Aulanier et al. 2005).

In previous studies, magnetic field evolution is typically assumed to be ideal (e.g., Isenberg & Forbes 2007 and references

therein). With no magnetic flux emerging or canceling between the photospheric sources (located at $x = \pm D$), this implies the conservation of the magnetic flux, F , through the area, S , defined between $z = 0$ and the bottom of the current channel. F is given by

$$F = \frac{L_e I}{2} + \iint_S B_{p,x} dy dz \tag{9}$$

$$= \frac{L_e I}{2} - 4\pi\phi \left(1 - \frac{D}{\sqrt{(h-a)^2 + D^2}} \right), \tag{10}$$

with $L_e = \mu_0 h (\ln 8h/a - 2)$ being the external inductance of the current channel (see Equation (1)). The conservation of F , together with the time evolution of one parameter of the model (e.g., ϕ or D) provides an evolution constraint with the generic form $I_{\text{evol.}}(h)$. Its intersection with the equilibrium curve, $I_{\text{eq.}}(h)$, determines the evolution of I as a function of the evolving parameter (e.g., ϕ or D).

With a circular current channel, Lin et al. (2002) has shown that evolving D with F preserved does not lead to a loss of equilibrium, but rather to a self-similar evolution of the configuration (which is just a rescale in size). However, they also show that a decrease in ϕ does lead to a loss of equilibrium. Figure 2(a) is a graphical representation of this result. As in previous studies, the maximum of $I_{\text{eq.}}(h)$ defines the reference state with fluxes ϕ_0 and F_0 . The evolution is parameterized by f_ϕ defined by $\phi = f_\phi \phi_0$, where f_ϕ is a decreasing function of time as observed after the emerging phase of an active region (e.g., van Driel-Gesztelyi et al. 2003) or before the filament eruption (e.g., Schmieder et al. 2008). In order to have an equilibrium curve not evolving with ϕ (to simplify the graphic),

we draw $I_{\text{eq.}}/\phi$ (normalized to its maximum value) as well as $I_{\text{evol.}}/\phi$.

Starting the evolution with $f_\phi > 1$, the constraint $F = F_0$ has an intersection with the equilibrium curve before its maximum (e.g., at the point “a” for $f_\phi = 1.5$ in Figure 2(a)). This equilibrium is stable since the perturbed equilibrium, with the constraint $F = F_0$, has a restoring force as shown with the arrows (see Section 4.1 for the analysis of the perturbed equilibrium).

As f_ϕ decreases (due, e.g., to magnetic flux cancellation with some photospheric flux brought from $|x| > D$), the equilibrium height h also increases. Contrary to what is obtained if the evolution of I is prescribed as in a circuit model, the conservation of magnetic flux in ideal MHD leads to the equilibrium still being stable after the maximum of $I_{\text{eq.}}/\phi$ (point “b”) up to point “c”.

For larger h values, e.g., at point “a’ ”, the equilibrium is unstable to an ideal perturbation (i.e., with F preserved). However, this unstable region is not reachable during the pre-eruptive evolution: the quasi-static evolution ends at point “c” with both equilibria becoming unstable (see arrows in Figure 2(a)) and without neighbor equilibrium as f_ϕ is slightly more increased, so there is loss of equilibrium. The evolution sequence with decreasing f_ϕ ends with a fast evolution driven by an outward force, and so an eruption occurs. It could be confined if a stable equilibrium is present at a greater height, e.g., due to the formation of a long current sheet below the flux rope (Forbes & Isenberg 1991), or if a too strong magnetic tension of the overlying field is present (as for the kink-unstable eruption modeled by Török & Kliem 2005).

3.3. Other Possible Evolutions on Intermediate Timescales

The analysis of the previous section assumes an ideal-MHD evolution to progressively shift the equilibrium to a point in the equilibrium curve where no neighbor equilibrium exists (with the magnetic flux conservation). This is only one plausible scenario for solar eruptions (see Section 1). Indeed, on the intermediate timescale τ_B , magnetic reconnection can play a crucial role in transforming the coronal field. For example, this is the case with a progressive diffusion of photospheric magnetic polarities leading to reconnection at the PIL and the transformation of sheared to twisted field lines contributing to buildup of the twisted flux tube and the associated current channel (as in the numerical simulations of Amari et al. 2003; Fan & Gibson 2004; Mackay & van Ballegooijen 2006; Aulanier et al. 2010). A progressive transformation of the coronal magnetic configuration is also expected due to the reconnection of the current layers formed at separatrices and quasi-separatrix layers (QSLs; e.g., Titov et al. 2002) during the intermediate timescale τ_B . We conclude that it is typically not obvious to justify an ideal-MHD evolution during the long pre-eruptive buildup phase before an eruption, on timescales much longer than τ_A , and in particular using the evolution constraint of a preserved flux below the flux rope (e.g., Equation (10)).

Generally, for a given observed configuration or in a three-dimensional MHD simulation, it is difficult to determine the main evolutionary constraint, even with a detailed analysis (e.g., Aulanier et al. 2010). This is not due to the lack of available data; rather, the difficulty is due to the complexities inherent in the three-dimensional evolution of magnetic fields. This is illustrated by the formidable complexity of studying the loss of equilibrium even in a simplified configuration (e.g., a small bipole emerging in a bipolar field; Lin et al. 2001).

3.4. Instability with a Circular Current Channel

Let us illustrate another possible evolution instead of the ideal-MHD evolution on the timescale τ_B . The following case is selected mainly because of its simplicity in illustrating other possible evolutions. The current channel is associated with a twisted flux tube that has a finite twist due to the presence of an axial magnetic field. The average coronal twist, T , is approximately related to the current I and the toroidal flux, ϕ_t , in the flux rope by (see Equation (9) in Titov & Démoulin (1999))

$$T = \mu_0 I h / (2\phi_t). \quad (11)$$

Let us suppose that the flux rope twist T is increasing, e.g., due to torsional Alfvén waves coming from the convective zone or as a consequence of reconnecting sheared loops (increasing the flux rope flux). Equation (11) provides a new evolution constraint replacing the conservation of F used in Section 3.2. As above, the maximum of $I_{\text{eq.}}(h)$ defines the reference state with the flux ϕ_0 and the twist T_0 . Here, we simply suppose that the photospheric field sources are not evolving, so $\phi = \phi_0$, but we still plot $I_{\text{eq.}}/\phi$ to be consistent with the previous case. The evolution is parameterized by f_T , defined by $T = f_T T_0$.

Starting the evolution with $f_T < 1$, the evolution constraint, Equation (11), has an intersection with the equilibrium curve before its maximum (e.g., at the point “a” for $f_T = 0.5$ in Figure 2(b)). As in Section 3.2, this equilibrium is stable. As f_T increases, the equilibrium height h also increases, reaching point “b” and then “c”. If we only consider the evolution constraint, the evolution would reach point “d”, where no neighbor equilibrium is present when f_T is further increased. As in the previous case (in Figure 2(a)), a loss of equilibrium is present but at a larger height.

However, the true physical evolution of the system ends earlier, at point “c”, where the system is unstable on the short timescale τ_A with an ideal-MHD perturbation (the preservation of the flux F in Equation (10)), while the evolution of T is negligible on the short timescale τ_A .

3.5. Loss of Equilibrium or Instability?

In the two previous evolutions (Figures 2(a) and (b)), the eruption occurs at the same location along the equilibrium curve, at point “c”. However, they appear to have a different theoretical origin. In the first case (Figure 2(a)), the progressive decrease of f_ϕ brings the system to point “c” where no neighbor equilibrium exists with a further decrease of f_ϕ . In the second case (Figure 2(b)), the increase of f_T also brings the system to point “c”, but a neighbor equilibrium is present with a further increase of f_T (up to point “d”). Simply put, the equilibrium after point “c” is unstable with an ideal perturbation (F preserved), and, as in the first case, an upward eruption is present after the system reaches point “c”. Indeed, on the timescale τ_A , the evolution of the two cases will be the same after they reach point “c”, since the same unstable force (Equation (6)) is acting with the constraint of an ideal-MHD evolution (and so preserving F in Equation (10)). We then argue that there is no point in discussing whether there is a loss of equilibrium or a transition from a stable to an unstable equilibrium.

Generally, for an observed coronal field evolution and even for an MHD simulation (where all the physical quantities are available in the volume), we claim that in most cases, it will be at least difficult, if not impossible to precisely define the evolution constraint as in the previous two cases. Indeed, with a slow enough driving, the system follows the equilibrium

curve, and the extensions away from this curve, along the evolution constraint, are purely theoretical considerations that are available only if an analytical analysis is achievable. In a magnetic configuration that includes some separatrices or QSLs, with some reconnection, we claim that an evolution constraint cannot be constructed generically. However, a generic approach is to test the ideal-MHD stability all along the evolution (within the limit of numerical dissipation for MHD simulations).

Because of the separation of the timescale of the coronal evolution (τ_A) from the longer timescales of the photospheric evolution (τ_B , τ_C ; see Section 3.1), the magnetic configuration cannot reach the equilibrium branch at an altitude h higher than that of point “c” by a slow quasi-static evolution, which does correspond to observed pre-eruptive evolutions. Reaching a region of the equilibrium curve beyond “c” may be dynamically possible, but only for fast (e.g., Alfvénic) evolutions of the magnetic configurations that are out of equilibrium. This is, however, not observed in the Sun’s atmosphere, even during flux emergence. Nevertheless, considering an analytical model of the equilibrium, one can always start a numerical simulation from any point along the equilibrium curve, stable or unstable (e.g., Török & Kliem 2007). The unstable branch is inaccessible for a coronal field, except the vicinity of point “c,” which can be reached with a small but finite velocity due to the slow evolution present in the pre-eruptive stage. Indeed, including such small velocity results in an evolution curve, $h(t)$, that is in better agreement with the observed $h(t)$ in prominence eruptions as opposed to the evolution curve obtained from letting the instability grow from an initial very small perturbation (Schrijver et al. 2008).

3.6. Loss of Equilibrium with a Straight Current Channel

The evolution summarized in Figures 2(a) and (b) is expected to be generic for magnetic configurations that have at least one current channel which is not fully neutralized since the hoop force is generally present in a curved current channel (Garren & Chen 1994). Indeed, this has been shown in more complex configurations, even when including a complete photospheric line tying, i.e., not only fixing the “normal magnetogram” (with the inclusion of image current; see Section 2.2), but also fixing the photospheric positions of the current channel (Isenberg & Forbes 2007).

However, the above physical evolution is not limited to the presence of the hoop force. It is indeed true of the Lorentz force created by any current channel. At a given position of the circuit, the magnetic force can be dominated either by the magnetic field created by the current located in the vicinity of this position (hoop force) or by the current at a large distance (e.g., an image current). Indeed, van Tend & Kuperus (1978) first proposed a catastrophe model of a straight current channel embedded in a potential field.

As in Section 3.2, a potential field \mathbf{B}_p is introduced to achieve equilibrium. As above, we select a bipolar field \mathbf{B}_p created by two magnetic sources of flux ϕ located at $x = \pm D$, $z = 0$, but now invariant by translation in the y -direction. The x -component of \mathbf{B}_p at the current location is

$$B_{p,x} = -2\phi D(\pi(h^2 + D^2))^{-1}. \quad (12)$$

The equilibrium current I_{eq} is given by $f = 0$ in Equation (6):

$$I_{\text{eq}}(h) = \frac{8\pi}{\mu_0} \frac{\phi Dh}{h^2 + D^2}. \quad (13)$$

The equilibrium curve is very similar to the one found for a circular current channel (compare panels (a) and (c) of Figure 2). The main difference is that the maximum of I_{eq} is shifted to a larger height. This is mainly due to the different dependence of $B_{p,x}$ on h for a two- and a three-dimensional bipole. Much closer equilibrium curves are obtained when the two-dimensional bipole is replaced by a two-dimensional quadrupole (giving a potential-field dependence similar to Equation (7)).

The conservation of the magnetic flux below the current channel, per unit length along its axis (Equation (9)), for the straight channel case is

$$F = \frac{\mu_0 I}{2\pi} \ln \frac{2h}{a} - \frac{2\phi}{\pi} \tan^{-1} \frac{h-a}{D}. \quad (14)$$

A major difference in the circular case is that the constraint of F conservation implies that I has a much weaker dependence on h (Figure 2(c)). It implies that the ideal-MHD instability occurs just after the maximum of I_{eq}/ϕ (where $f_\phi = 1$), when the photospheric polarities have weakened by only 4% ($f_\phi = 0.96$). Indeed, the ideal-MHD evolution leads to non-equilibrium at a location close to the one found by van Tend & Kuperus (1978) with the evolution simply driven by an increase in the current I .

As for the circular current channel, loss of equilibrium at point “c” is only present if the magnetic evolution is fully ideal. Generally, whatever the driver of the evolution on the timescale τ_B , the system is becoming unstable as it reaches point “c,” and it is ideally driven away from the equilibrium curve by the same force in the short timescale τ_A .

3.7. Comparison to Previous Studies

Based on our analysis above, we can now answer the following question: is there a major difference between the following approaches: the “loss of equilibrium” studies with straight or circular current channel (e.g., van Tend & Kuperus 1978; Lin et al. 2002) and the “torus instability” (Kliem & Török 2006) previously studied in the tokamak laboratory experiment (e.g., Bateman 1978)?

First, the straight or circular current channels have very similar repulsion forces, $r(h)I^2$, implying the same kind of equilibrium curve. Indeed, for a circular current channel, $r_c(h)$ has a contribution from both the coronal part ($z > 0$) and the image current ($z < 0$). Both contributions can be combined in a single term, Equation (4), masking the contribution of the image current. In a more general case, Garren & Chen (1994) have derived a general expression for $r(h)$ for arbitrary current shapes; r_c and r_s (Equations (4) and (5)), are simply two limits of the same $r(h)$, for circular and straight current channels.

Next, Kliem & Török (2006) studied the “torus instability” of a circular current channel imposing a constant current I or a constant flux F . The first case is directly comparable to the work of van Tend & Kuperus (1978) and the second case to the work of Lin et al. (2002). The only significant difference is that Kliem & Török (2006) study the stability of the equilibrium curve (Figure 2(a)) but do not follow the evolution of the magnetic configuration on the intermediate timescale τ_B (so they cannot detect the presence or absence of a loss of equilibrium).

The main difference between the loss of equilibrium and the stability analysis is that, for the first case, a precise way of how the system can evolve to instability is proposed, while in the second case, one only tests the stability of a given equilibrium (which could be physically inaccessible). However, for both type of analyses, an ideal instability is present at the same location in

the equilibrium curve if the same equilibrium is analyzed. This last condition is not trivial if one allows the formation of current sheets during the long-term evolution (on the timescale τ_B).

4. EQUILIBRIUM STABILITY

We study below the stability of the magnetic configuration around an equilibrium position. The main *assumption* is that the magnetic force balance is the same at any position along the current channel, so that the magnetic force can be written as in Equation (6). This includes both circular and straight current channels in the same formalism. The stability of the configuration is first derived in this general framework in Section 4.1, with the constraint of magnetic flux conservation derived in Section 4.2. These results are used in the particular cases studied in the previous section. Finally, a parametric study of the stability is presented.

4.1. Force Perturbation

The magnetic force, $f(a, h, I)$, on the current channel is described by Equation (6). A perturbation (da, dh, dI) around the equilibrium, $f(a, h, I) = 0$, creates the force df as

$$df = \frac{\partial f}{\partial a} da + \frac{\partial f}{\partial h} dh + \frac{\partial f}{\partial I} dI. \quad (15)$$

During the perturbation, the radius a evolves as given by the internal force balance. With a linear force-free field inside the flux rope and ideal MHD, Lin et al. (1998) found that a evolves as $1/I$. Here we include a more general variation, supposing $a(I)$, and we introduce the index of variation of a with I :

$$n_a \equiv -\frac{\partial \ln a}{\partial \ln |I|}; \quad (16)$$

$n_a = 1$ for the internal evolution included in Lin et al. (1998). Then, Equation (15) is rewritten as

$$df = \left(\frac{\partial f}{\partial h} + \left(-n_a \frac{a}{I} \frac{\partial f}{\partial a} + \frac{\partial f}{\partial I} \right) \frac{dI}{dh} \Big|_{\text{pert.}} \right) dh, \quad (17)$$

where $dI/dh|_{\text{pert.}}$ expresses how the current intensity is modified during the perturbation.

If the perturbation is realized along the equilibrium curve, the force df has the same expression, except that $dI/dh|_{\text{eq.}}$, computed along the equilibrium curve, replaces $dI/dh|_{\text{pert.}}$ in Equation (17). Also in this case, $df = 0$, so

$$\frac{\partial f}{\partial h} + \left(-n_a \frac{a}{I} \frac{\partial f}{\partial a} + \frac{\partial f}{\partial I} \right) \frac{dI}{dh} \Big|_{\text{eq.}} = 0, \quad (18)$$

where we suppose that the internal equilibrium has the same n_a index. Using the equilibrium condition $f = r I^2 + B_{p,x} I = 0$ and Equation (18), Equation (17) is rewritten as

$$df = r I \left(1 - n_a \frac{\partial \ln r}{\partial \ln a} \right) \left(\frac{dI}{dh} \Big|_{\text{pert.}} - \frac{dI}{dh} \Big|_{\text{eq.}} \right) dh. \quad (19)$$

The equilibrium is unstable when df and dh have the same signs. Thus, an instability is present when the absolute value of the current in the perturbation decreases less rapidly with height than along the equilibrium curve. This is illustrated in Figure 2.

On the short timescale τ_A , the perturbation is described by an ideal MHD, with preservation of the flux distribution at the boundary $z = 0$ (so $\phi = \text{constant}$ in the examples of Sections 3.2 and 3.6). Then, a perturbation corresponds to a small excursion away from the equilibrium curve with the constraint of magnetic flux conservation in Figures 2(a) and (c). The tangent point “c” between the equilibrium curve and the constraint of flux conservation define both the limit of the stable region and the non-equilibrium point (in an ideal evolution on the timescale τ_B).

Using the equilibrium condition to specify $dI/dh|_{\text{eq.}}$, the force perturbation, Equation (17), is rewritten as

$$\frac{df}{dh} = r I \left(1 - n_a \frac{\partial \ln r}{\partial \ln a} \right) \frac{dI}{dh} \Big|_{\text{pert.}} + I \frac{\partial B_{p,x}}{\partial h} + I^2 \frac{\partial r}{\partial h}. \quad (20)$$

We define the decay index of the potential field as

$$n_{Bp} \equiv -\frac{\partial \ln |B_{p,x}|}{\partial \ln h}. \quad (21)$$

This decay index is introduced in Equation (20) by dividing df by $B_{p,x} I$, or equivalently by $-r I^2$, and by multiplying by h . Finally, the equilibrium is unstable (i.e., $df/dh > 0$) if

$$\begin{aligned} n_{Bp} > n_{Bp,\text{crit.}} &\equiv n_r + n_1 \\ &\equiv -\frac{\partial \ln r}{\partial \ln h} - \left(1 - n_a \frac{\partial \ln r}{\partial \ln a} \right) \frac{d \ln |I|}{d \ln h} \Big|_{\text{pert.}}, \end{aligned} \quad (22)$$

if the potential field decreases fast enough with height. The instability threshold depends on how fast the repulsion decreases with height (given by the decay index n_r) and on how much the current is allowed to decrease during the perturbation (given by the decay index n_1).

4.2. Constraint of Flux Conservation

The decay index n_1 is computed from an ideal MHD constraint as follows. On the short timescale τ_A , the perturbation is described by ideal MHD, with the preservation of the coronal magnetic flux F present below the flux rope. With a small perturbation dh , Equation (9) implies

$$dF = \left(\frac{dL_e}{dh} I + L_e \frac{dI}{dh} \Big|_{\text{pert.}} + P B_{p,x} \right) \frac{dh}{2} = 0, \quad (23)$$

where P is the perimeter (or length) of the full current channel, including its image.

The external inductance L_e (computed with $l_i = 0$) depends generally on the spatial extension of the current channel (described here only by h) and on the thickness of the current channel (its radius a). Then, the variation of the external inductance with height is

$$\begin{aligned} \frac{dL_e}{dh} &= \frac{\partial L_e}{\partial h} + \frac{\partial L_e}{\partial a} \frac{\partial a}{\partial I} \frac{dI}{dh} \Big|_{\text{pert.}} \\ &= \frac{\partial L_e}{\partial h} - n_a L_e \frac{\partial \ln L_e}{\partial \ln a} \frac{d \ln |I|}{dh} \Big|_{\text{pert.}}. \end{aligned} \quad (24)$$

The conservation of the magnetic flux, Equation (23), together with Equation (24), implies the following decay index:

$$n_1 = \frac{1 - n_a \frac{\partial \ln r}{\partial \ln a}}{1 - n_a \frac{\partial \ln L_e}{\partial \ln a}} \left(\frac{\partial \ln L_e}{\partial \ln h} - \frac{P h r}{L_e} \right). \quad (25)$$

The last factor in Equation (25) is due to the conservation of the magnetic flux from the current I minus the flux from the potential field passing below the current channel. The fraction includes the effect of the channel expansion on the repulsion function at the numerator and on the conservation of flux at the denominator. The numerator and the denominator are both larger than 1 for $n_a > 0$, and they are a growing function of n_a . Then, the dependence of r and L_e on a have opposite effects on the stability.

4.3. Example of a Circular Current Channel

We apply the above results to a circular current channel in this subsection (Figure 1(b)). The external inductance L_e is given by Equation (1) without the contribution of the internal inductance ($l_i = 0$). The repulsion r is given by Equation (4) and $P = 2\pi h$. The contribution from the potential field to the decay index n_1 is (for $n_a = 0$, i.e., for a constant during the evolution)

$$-\frac{P h r}{L_e} = -\frac{1}{2} \left(1 + \frac{1 + l_f/2}{\ln(8h/a) - 2} \right). \quad (26)$$

The contribution from the field created by the current channel to the decay index n_1 is (for $n_a = 0$)

$$\frac{\partial \ln L_e}{\partial \ln h} = 1 + \frac{1}{\ln(8h/a) - 2}, \quad (27)$$

which is exactly twice the negative contribution from the potential field for $l_f = 0$. For $a \ll h$, i.e., a very thin current channel, the denominator, $\ln(8h/a) - 2$, is relatively large so that the above contributions are close to $-1/2$ and $+1$, respectively. Including Equations (26) and (27) in Equation (25) and using Equation (1), the decay index n_1 for the circular current channel is

$$n_1 = \frac{(u + l_f/2 + n_a)(u - l_f/2)}{2(u - 1 + n_a)(u + l_f/2)}, \quad (28)$$

with the notation

$$u = \ln(8h/a) - 1. \quad (29)$$

Using Equation (4), the decay index of the repulsion r is

$$n_r = -\frac{\partial \ln r}{\partial \ln h} = 1 - \frac{1}{u + l_f/2}. \quad (30)$$

From Equation (22), n_r is the critical decay index of \mathbf{B}_p for instability if the current I is preserved during the perturbation. n_r is always lower than 1, especially for a flux rope with large radius a .

Combining the results of Equations (28) and (30), the instability condition for a circular current channel is

$$n_{\text{Bp}} > \frac{3}{2} - \frac{(1 + l_f/2)(u - 2 + 2n_a + l_f/2)}{2(u + l_f/2)(u - 1 + n_a)}. \quad (31)$$

In the limit of a very thin current channel ($a \ll h$), the instability threshold is close to $3/2$, as found in tokamak studies (e.g., Bateman 1978). This corresponds to the ‘‘torus instability’’ for solar eruptions (Kliem & Török 2006), but with a different correction term than $3/2$, as we have not supposed a self-similar expansion of the current channel, but rather a dependence $a(I)$.

4.4. Example of a Straight Current Channel

We follow the same derivation as in the previous subsection for a current channel formed by two parallel lines (Figure 1(c)). In this geometry, the external inductance L_e is given by Equation (2), again with $l_i = 0$. The repulsion r is given by Equation (5) and $P = 2\Delta y$ (with $\Delta y \gg h, D$). For $n_a = 0$, the contribution from the field created by the current channel to the decay index n_1 , Equation (25), is exactly twice the contribution from the potential field, but with the opposite sign (as above for the circular channel with $l_f = 0$):

$$\frac{\partial \ln L_e}{\partial \ln h} = 2 \frac{P h r}{L_e} = \frac{1}{\ln(2h/a)}. \quad (32)$$

With Equation (5), the decay index of the repulsion r is simply $n_r = 1$. Combining the above results, the instability condition, Equation (22), for a straight current channel is

$$n_{\text{Bp}} > 1 + \frac{1}{2(\ln(2h/a) + n_a)}. \quad (33)$$

In the limit of a very thin current channel ($a \ll h$), the instability threshold is close to 1, as found by van Tend & Kuperus (1978).

4.5. Comparison of Circular and Straight Current Channels

From Equation (22), the critical decay index of the potential field for instability, $n_{\text{Bp,crit}}$, has two contributions: the decay indices of the repulsion, n_r , and the decay index of the current during the ideal perturbation, n_1 . The main difference of stability between the above two current channels is a much lower index n_1 for the straight channel (Figure 3). This is due to the weak dependence of L_e on the height h (compare Equation (2) to Equation (1)). At the limit $a \ll h$, a circular current channel is more stable ($n_{\text{Bp,crit}} \approx 3/2$) than a straight current channel ($n_{\text{Bp,crit}} \approx 1$). However, this limit is not applicable to the eruptive coronal configurations since it requires extremely thin current channels: for example, even with $a/D = 10^{-3}$, this limit is only weakly approached (Figure 4). This is due to the $\ln(h/a)$ dependence in both Equations (31) and (33).

Moreover, the above difference is partly compensated by a lower decay index of the repulsion, n_r , for a circular channel (as the repulsion, $r(h)$, is decreasing slower with height, especially for large values of a). The net result is that the critical decay indices, $n_{\text{Bp,crit}}$, for circular and straight channels, with finite radius a , are much closer than in the limit $a \ll h$. This is illustrated in Figure 3 with $a/D = 0.1$, which still corresponds to a relatively narrow channel. This effect is amplified with a flux rope having a larger expansion during the perturbation, and hence a larger n_a value, because the contribution of n_1 to $n_{\text{Bp,crit}}$ is reduced. Indeed, even with a relatively thin flux rope, $a/D = 0.1$, and an internal expansion rate $n_a = 1$, as in Lin et al. (1998), $n_{\text{Bp,crit}}$ values are close for circular and straight current channels: ≈ 1.3 and ≈ 1.1 , respectively (Figures 3(c) and (d)). They correspond to a comparable critical height ($h/D \approx 1$) for straight and circular channels with a two- and a three-dimensional bipole (Equations (7) and (12), respectively).

In the previous studies, the instability threshold $n_{\text{Bp,crit}}$ was typically taken in the limit of very thin current channels (e.g., van Tend & Kuperus 1978; Kliem & Török 2006). The above analytical theory is indeed done in the limit of thin current channels (typically $a/D \leq 0.1$). In fact, relatively broad current channels are expected in the corona with magnetic extrapolations (e.g., Schrijver et al. 2008; Savcheva & van

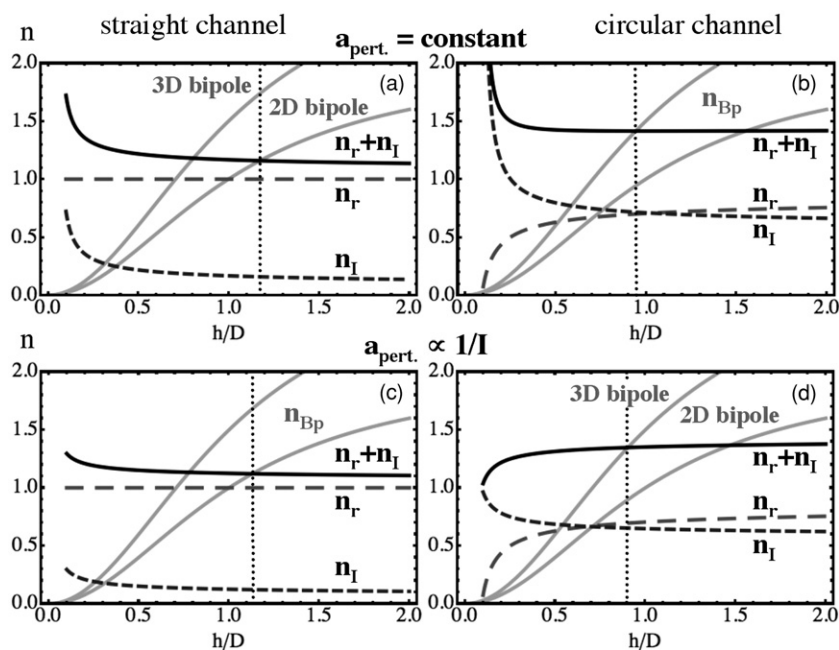


Figure 3. Dependence of the decay indices $n_r = -\partial \ln r / \partial \ln h$, $n_I = -\partial \ln |I| / \partial \ln h$, and $n_{Bp} = -\partial \ln |B_{p,x}| / \partial \ln h$ for a straight (circular) current channel in the left (right) column. The critical index $n_{Bp,crit.} = n_r + n_I$ for instability is shown with a black continuous line. The decay indices of two- and three-dimensional potential bipoles are shown in both columns for reference. The dotted vertical line indicates the critical height (point “c” in Figure 2). All panels are drawn with the normalized equilibrium radius $a/D = 0.1$ and for $h > a$. The top (bottom) panels have $n_a = -\partial \ln a / \partial \ln |I| = 0$ ($n_a = 1$).

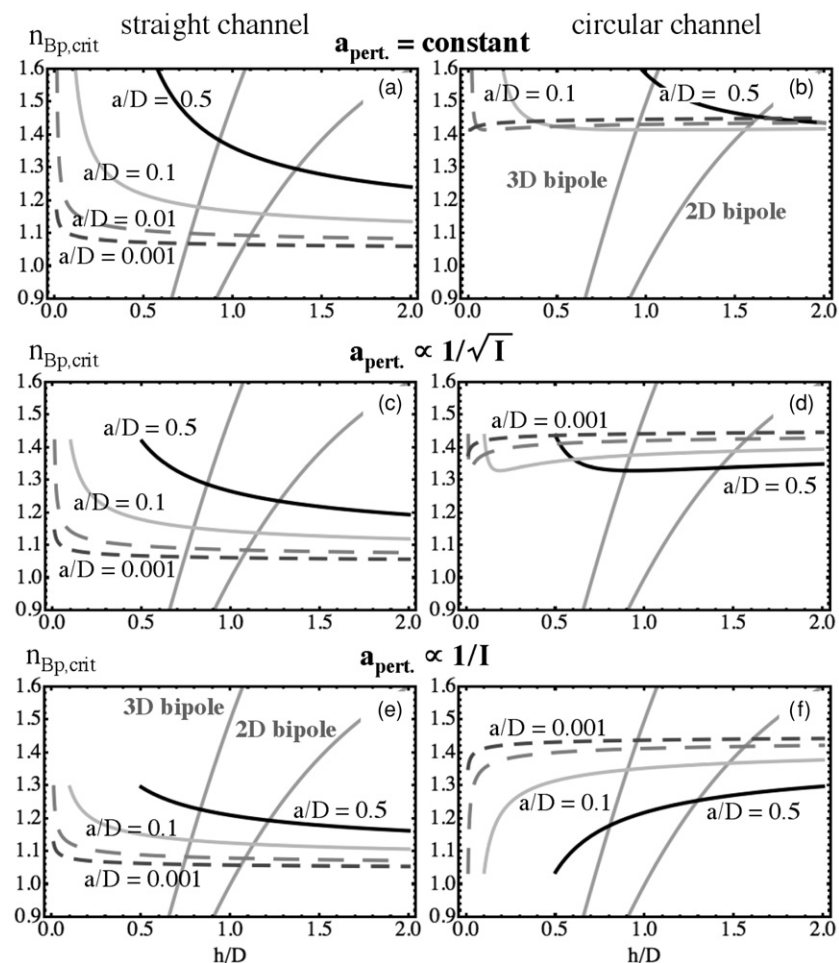


Figure 4. Critical index $n_{Bp,crit.} = n_r + n_I$ for instability with various equilibrium radii a normalized by D (half distance between photospheric field concentrations). The results are for a straight (circular) current channel in the left (right) column. The flux rope expands more during the perturbation (larger n_a value) from top ($n_a = 0$) to bottom ($n_a = 1$). The $n_{Bp,crit.}$ curves are drawn for $h > a$. The decay indices, n_{Bp} , of two- and a three-dimensional potential bipole are shown in both columns for reference.

Ballegooijen 2009) and are present in MHD simulations (e.g., Fan & Gibson 2004; Török & Kliem 2007; Aulanier et al. 2010). So, we also show the approximative results for a broad channel case, $a/D = 0.5$. For a straight current channel, the flux conservation provides an increasing stabilizing effect as the channel radius, a , increases (Figure 4). Indeed, for a broad *straight* channel ($a/D \geq 0.1$), $n_{\text{Bp,crit.}}$ can reach a value comparable to, or even larger in some cases, than the one obtained for the corresponding circular channel with the same parameter values (Figures 4(e) and (f)). We conclude that the circular and straight current channels have typically comparable instability threshold values for the range of parameters expected in the corona.

The internal evolution of the current channel during the perturbation (i.e., the effect of n_a) has a common effect on the stability of a circular and of a straight current channel because the stabilizing term provided by the flux conservation generally decreases with an increase in n_a (Figures 3 and 4). However, changing the channel thickness (a/D) has the opposite effect on the instability threshold for a circular and for a straight current channel (compare the panels in Figure 4, where the a/D curves are ordered oppositely in the two columns). For a straight channel, $n_r = 1$, and so $n_{\text{Bp,crit.}} = n_r + n_l$ is affected only by the dependence of n_l on a/D . But, as soon as n_a is slightly positive, for a circular channel, the n_r dependence on a/D is important and dominates the contribution of n_l . It implies a dependence of $n_{\text{Bp,crit.}}$ on a/D for a circular channel that is opposite to that for a straight channel.

5. CONCLUSION

How to destabilize a coronal magnetic configuration is a key issue of CME research. Loss of equilibrium and torus instability occurring during the evolution of the magnetic configuration are two candidates among several possible ones. Both have been initially developed with the approximation that the coronal currents are restricted to a non-neutralized current channel, and both theories were further analyzed via MHD simulations, relaxing part of the initial approximations of the analytical developments, but at the expense of not covering the entire parameter space.

In this study, we revisit both analytical theories and compare their approaches to the two simple configurations where their results apparently differ: a straight and a circular current channel. Loss of equilibrium is typically, but not always, present in both configurations when an ideal-MHD evolution is imposed during the long-term evolution of the magnetic configuration. However, when a loss of equilibrium occurs, the magnetic configuration is also ideally unstable. From the results of Sections 3 and 4, we conclude that both approaches are in fact both compatible and complementary. In particular, they agree on the position of the instability if no significant current sheets are formed during the long-term evolution of the magnetic configuration. Moreover, slow resistive processes, e.g., tether cutting, are probably occurring all throughout before an eruption occurs. Therefore, we conclude that analytical theory is most useful in deriving an instability threshold with the constraint of ideal MHD evolution on a short timescale (coronal Alfvén time) for a given magnetic equilibrium.

We also compare the physical origin of the instability of straight and circular current channels. In order to model the negligible evolution of the magnetic flux crossing the photosphere on the coronal Alfvén timescale, a theoretical image

current is introduced below the photosphere (Figure 1). For a straight current channel, the repulsion of the image balances the Laplace force between the coronal current and the potential field (associated with the photospheric field distribution). For a circular current channel, the repulsion of the nearby coronal current (called hoop force) is also present. However, since the repulsion force depends only on the global curvature radius and on the thickness of the current channel for the circular channel, it could lead to the false conclusion that the repulsion force has a different origin for the straight and circular current channels. In fact, as shown by Garren & Chen (1994), both the coronal and the image currents generally contribute to the repulsion force of a current channel. Both terms actually combine in a single expression for a circular channel, while there is no contribution from the coronal current for a strictly straight current channel. The circular and straight current channels are simply two limits of the general case with specific properties.

Instability occurs when the potential magnetic field decreases fast enough with height; more precisely, when its decay index, n_{Bp} , as defined by Equation (21), is larger than a critical value $n_{\text{Bp,crit.}}$. At the limit of extremely thin current channels, $n_{\text{Bp,crit.}} = 1$ and 1.5 for a straight and circular current channel, respectively. Further, we show that this difference is not due to the difference in the repulsion force, but due to the constraint of ideal MHD (the conservation of the coronal magnetic flux below the current channel). Moreover, when the repulsion force is the sole contributor to the instability threshold (i.e., $n_l = 0$ in Equation (22)), then first, $n_{\text{Bp,crit.}} < 1$ for a circular current channel while $n_{\text{Bp,crit.}} = 1$ for a straight channel, and second $n_{\text{Bp,crit.}}$ approaches 1 for both circular and straight channel as the channel becomes very thin. This further indicates that there is no real difference in the origin of the repulsion force for the straight and circular current channel.

We conclude that the same physics is involved in the instability of circular and straight current channels, and that they are just two particular limiting cases of more general current paths. For the typical range of current-channel thickness expected in the corona and present in MHD simulations, and for a current channel expanding during an upward perturbation, $n_{\text{Bp,crit.}}$ has close values for both the circular and straight current channels (in the range [1.1, 1.3]; Figures 4(e) and (f)). If the current channel would not expand, the decay index $n_{\text{Bp,crit.}}$ would be higher, typically in the range [1.2, 1.5], but would still not be very different in both cases (Figures 4(a) and (b)). Similar critical indices have been found in MHD simulations that start from an initial equilibrium having a coronal current channel close to half torus (Török & Kliem 2007; Schrijver et al. 2008). Otherwise, from the measurement of the height of a set of quiescent prominences, combined with potential field extrapolations, Filippov & Den (2001) found $n_{\text{Bp,crit.}} \approx 1$. This threshold is closer to the $n_{\text{Bp,crit.}}$ of the straight current channel as expected since quiescent prominences are horizontally extended structures.

In an MHD simulation, where a flux rope and its associated current channel is progressively formed due to photospheric motions, flux cancellation, and magnetic reconnection, Aulanier et al. (2010) found an unstable configuration when $n_{\text{Bp,crit.}} \approx 1.5$. There, the flux rope height satisfied $h/D \approx 1$. This was in favor of the “torus instability.” However, with the above results, this threshold would require that the current channel is almost rigid during the perturbation (i.e., $n_a = 0$ as in Figure 4(b)). It is not obvious that this condition is met in a low- β magnetic field. The role of the anchorage of the current

channel at fixed photospheric positions during the stability analysis, a constraint not present for both the straight and circular models studied above, but included in the non-equilibrium study of Isenberg & Forbes (2007) is probably more relevant. The present analytical theory also over simplifies the coronal current distribution to only one current channel, while at least partial current neutralization as well as other current layers are typically present in MHD simulations. This may also raise the critical index, $n_{Bp,crit.}$, to larger values (e.g., $n_{Bp,crit.}$ as high as 1.9 was found in the MHD simulations of flux emergence by Fan & Gibson 2007). The precise understanding of the instability threshold is important for determining when a CME would occur. This will be the object of further developments of the analytical theory.

It would also be desirable to derive the critical index from observations of eruptive prominences and sigmoids, the pre-eruptive altitudes of which can be measured either using two vantage points (e.g., using the pair of STEREO imagers) or when they cross the solar limb. At first approximation, the background coronal magnetic field would then have to be extrapolated from the potential field approximation using photospheric magnetograms either taken on the same day of the eruption if possible, or a few days before if no magnetogram is available. Such a survey of various eruptive solar features would extend the work carried out by Filippov & Den (2001), who focused on long and high altitude quiescent prominences that mostly concern the straight channel model.

The authors thank the referee for helpful comments, which improved the clarity of the paper. Financial supports by the European Commission through the FP6 SOLAIRE Network (MTRN-CT- 2006-035484) and through the FP7 SOTERIA project (Grant Agreement no 218816) are acknowledged.

REFERENCES

- Aly, J. J. 1985, *A&A*, **143**, 19
 Amari, T., & Aly, J. J. 1989, *A&A*, **208**, 261
 Amari, T., Luciani, J. F., Aly, J. J., Mikic, Z., & Linker, J. 2003, *ApJ*, **595**, 1231
 Amari, T., Luciani, J. F., Mikic, Z., & Linker, J. 2000, *ApJ*, **529**, L49
 Antiochos, S. K., DeVore, C. R., & Klimchuk, J. A. 1999, *ApJ*, **510**, 485
 Anzer, U., & Ballester, J. L. 1990, *A&A*, **238**, 365
 Aulanier, G., Démoulin, P., & Grappin, R. 2005, *A&A*, **430**, 1067
 Aulanier, G., Török, T., Démoulin, P., & DeLuca, E. E. 2010, *ApJ*, **708**, 314
 Bateman, G. 1978, *MHD Instabilities* (Cambridge, MA: Massachusetts Institute of Technology)
 Chen, J. 1989, *ApJ*, **338**, 453
 Démoulin, P., Ferreira, J., & Priest, E. R. 1991, *A&A*, **245**, 289
 Démoulin, P., & Priest, E. R. 1988, *A&A*, **206**, 336
 Fan, Y., & Gibson, S. E. 2004, *ApJ*, **609**, 1123
 Fan, Y., & Gibson, S. E. 2007, *ApJ*, **668**, 1232
 Filippov, B. P., & Den, O. G. 2001, *J. Geophys. Res.*, **106**, 25177
 Forbes, T. G. 2000, *J. Geophys. Res.*, **105**, 23153
 Forbes, T. G., & Isenberg, P. A. 1991, *ApJ*, **373**, 294
 Forbes, T. G., & Priest, E. R. 1995, *ApJ*, **446**, 377
 Forbes, T. G., et al. 2006, *Space Sci. Rev.*, **123**, 251
 Garren, D. A., & Chen, J. 1994, *Phys. Plasmas*, **1**, 3425
 Gibson, S. E., Fan, Y., Török, T., & Kliem, B. 2006, *Space Sci. Rev.*, **124**, 131
 Green, L. M., & Kliem, B. 2009, *ApJ*, **700**, L83
 Green, L. M., López fuentes, M. C., Mandrini, C. H., Démoulin, P., Van Driel-Gesztelyi, L., & Culhane, J. L. 2002, *Sol. Phys.*, **208**, 43
 Grover, F. W. 1946, *Inductance Calculations: Working Formulas and Tables* (New York: Dover)
 Isenberg, P. A., & Forbes, T. G. 2007, *ApJ*, **670**, 1453
 Isenberg, P. A., Forbes, T. G., & Démoulin, P. 1993, *ApJ*, **417**, 368
 Jackson, J. D. 1975, *Classical Electrodynamics* (2nd ed.; New York: Wiley)
 Kahler, S. W., Moore, R. L., Kane, S. R., & Zirin, H. 1988, *ApJ*, **328**, 824
 Kliem, B., & Török, T. 2006, *Phys. Rev. Lett.*, **96**, 255002
 Klimchuk, J. A., & Sturrock, P. A. 1989, *ApJ*, **345**, 1034
 Krall, J., Chen, J., & Santoro, R. 2000, *ApJ*, **539**, 964
 Kuperus, M., & Raadu, M. A. 1974, *A&A*, **31**, 189
 Lin, J., Forbes, T. G., & Isenberg, P. A. 2001, *J. Geophys. Res.*, **106**, 25053
 Lin, J., Forbes, T. G., Isenberg, P. A., & Démoulin, P. 1998, *ApJ*, **504**, 1006
 Lin, J., van Ballegooijen, A. A., & Forbes, T. G. 2002, *J. Geophys. Res.*, **107**, 1438
 Mackay, D. H., & van Ballegooijen, A. A. 2006, *ApJ*, **641**, 577
 Malmberg, J. H., & Rosenbluth, M. N. 1965, *Rev. Sci. Instrum.*, **36**, 1886
 Maričić, D., Vršnak, B., Stanger, A. L., Veronig, A. M., Temmer, M., & Roša, D. 2007, *Sol. Phys.*, **241**, 99
 Martens, P. C. H., & Kuin, N. P. M. 1989, *Sol. Phys.*, **122**, 263
 Moore, R. L., Larosa, T. N., & Orwig, L. E. 1995, *ApJ*, **438**, 985
 Moore, R. L., & Roumeliotis, G. 1992, in *IAU Colloq. 133, Eruptive Solar Flares*, ed. Z. Svestka, B. V. Jackson, & M. E. Machado (Lecture Notes in Physics, Vol. 399; Berlin: Springer), 69
 Neupert, W. M., Thompson, B. J., Gurman, J. B., & Plunkett, S. P. 2001, *J. Geophys. Res.*, **106**, 25215
 Parker, E. N. 1996a, *ApJ*, **471**, 489
 Parker, E. N. 1996b, *ApJ*, **471**, 485
 Ramo, S., Whinnery, J., & Van Duzer, T. 1994, *Fields and Waves in Communication Electronics* (3rd ed.; New York: Wiley)
 Savcheva, A., & van Ballegooijen, A. 2009, *ApJ*, **703**, 1766
 Schmieder, B., Bommier, V., Kitai, R., Matsumoto, T., Ishii, T. T., Hagino, M., Li, H., & Golub, L. 2008, *Sol. Phys.*, **247**, 321
 Schrijver, C. J., Elmore, C., Kliem, B., Török, T., & Title, A. M. 2008, *ApJ*, **674**, 586
 Shafranov, V. D. 1966, *Rev. Plasma Phys.*, **2**, 103
 Temmer, M., Veronig, A. M., Vršnak, B., Rybák, J., Gömöry, P., Stoiser, S., & Maričić, D. 2008, *ApJ*, **673**, L95
 Titov, V. S., & Démoulin, P. 1999, *A&A*, **351**, 707
 Titov, V. S., Hornig, G., & Démoulin, P. 2002, *J. Geophys. Res.*, **107**, 1164
 Török, T., & Kliem, B. 2003, *A&A*, **406**, 1043
 Török, T., & Kliem, B. 2005, *ApJ*, **630**, L97
 Török, T., & Kliem, B. 2007, *Astron. Nachr.*, **328**, 743
 van Ballegooijen, A. A., & Martens, P. C. H. 1989, *ApJ*, **343**, 971
 van Driel-Gesztelyi, L. 1998, in *ASP Conf. Ser. 155, Three-Dimensional Structure of Solar Active Regions*, ed. C. E. Alissandrakis & B. Schmieder (San Francisco, CA: ASP), 202
 van Driel-Gesztelyi, L., Démoulin, P., Mandrini, C. H., Harra, L., & Klimchuk, J. A. 2003, *ApJ*, **586**, 579
 van Tend, W., & Kuperus, M. 1978, *Sol. Phys.*, **59**, 115
 Venkatakrishnan, P., & Tiwari, S. K. 2009, *ApJ*, **706**, L114
 Vršnak, B. 2008, *Ann. Geophys.*, **26**, 3089
 Vršnak, B., Maričić, D., Stanger, A. L., & Veronig, A. 2004, *Sol. Phys.*, **225**, 355
 Wheatland, M. S. 2000, *ApJ*, **532**, 616
 Zhang, J., Dere, K. P., Howard, R. A., Kundu, M. R., & White, S. M. 2001, *ApJ*, **559**, 452